

Q matrix approach to control implant heating by transmit array coils

Frank Seifert¹, Gerd Weidemann¹, and Bernd Ittermann¹

¹Physikalisch-Technische Bundesanstalt (PTB), Braunschweig und Berlin, Germany

Target audience: Basic researchers interested in managing RF safety of metallic implants when using transmit array coils

Purpose: The hazard of excessive local tissue heating due to metallic implants can be mitigated when utilizing the additional degrees of freedom of a transmit coil array. In this proof of principle study we used the single Q matrix associated with the proximate tissue volume of a metallic implant to determine the 'worst case' steering conditions for implant heating. From a simple projection of the voltage vector to be applied to a sub space which is orthogonal to this 'worst case' voltage vector new steering conditions are determined which result in much lower implant heating. To demonstrate the efficacy of this method we performed thermal simulations using a 7T 8-channel head coil model. The approach can simply be embedded into B1-shimming procedures.

Methods:

Model: 7T 8-channel decoupled loop array with external shield using 'Ella' as head model, all tissue parameters for EM modeling are from the ITIS database^{2,3}. A thin perfectly conducting wire was 'implanted' in z-direction into the brain. Outside the head the wire was bent into x-direction (red arrow in Fig. 1).

EM simulations: XFDTD 6.4 (Remcom Inc.), equidistant mesh (2mm), 8 million FDTD cells, CW excitation, 3D data sets of complex valued E, H and J field vector amplitudes were extracted for each of the 8 driving and 16 decoupling ports.

Co-simulation: Tuning, matching and decoupling of coil elements were performed by using T-type matching circuits and decoupling capacitors. Intrinsic coil losses were included in the matching circuit by an additional resistor to achieve realistic quality factor ratios.

Field superposition: For each 8-component complex valued driving voltage vector $|u\rangle$ all electromagnetic field components (E, H and j) are calculated by superposition of all 24 3D field data sets using the complex valued weighting factors from co-simulation.

Implant Q matrix: The Q matrix of the implant $Q_{imp} = \langle j^* E \rangle_V$ was calculated by choosing an averaging volume V consisting of all FDTD cells adjoining the conductive outer boundary of the implant. In the case of a straight wire this volume is simply determined by all 3 by 3 FDTD cells along the implant.

Voltage vectors: We considered 4 different configurations: (i) $|u\rangle$ is given by the 'worst case' eigenvector $|u_{max}\rangle$ determined by the maximum eigenvalue of Q_{imp} . (ii) $|u\rangle = |u_{max}\rangle$, but EMF simulation with no implanted wire. (iii) CP-mode excitation $|u\rangle = |u_{CP}\rangle$, i.e. equal amplitudes, 45 degree phase increment per Tx-channel. (iv) $|u\rangle = |u_{CP}\rangle - |u_{max}\rangle \langle u_{max} | u_{CP} \rangle$ (assuming normalization $\langle u_{CP} | u_{CP} \rangle = \langle u_{max} | u_{max} \rangle = 1$), i.e. $|u\rangle$ is always orthogonal to $|u_{max}\rangle$.

Thermal modelling: Pennes' Bioheat Equation¹ was implemented on exactly the same FDTD mesh as the EMF calculation using the OpenACC framework of the PGI compiler suite (The Portland Group, Beaverton, OR) for GPU acceleration. Steady state temperatures were assumed to be reached after 1 hour of heating. Maximum steady state temperatures were determined for the position of the wire's tip (T_{tip}) and for the CSF - grey matter boundary nearby the implant (T_{csf}). Furthermore, we neglected thermal conductivity of the implant which is a conservative assumption. Tissue specific values of density, heat capacity, thermal conductivity, metabolic heat generation rate and blood perfusion rate were taken from the ITIS database². For thermal simulations total forward RF power was 20W.

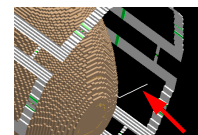
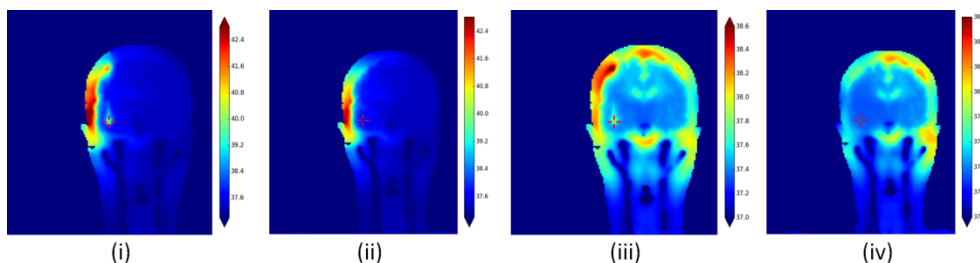
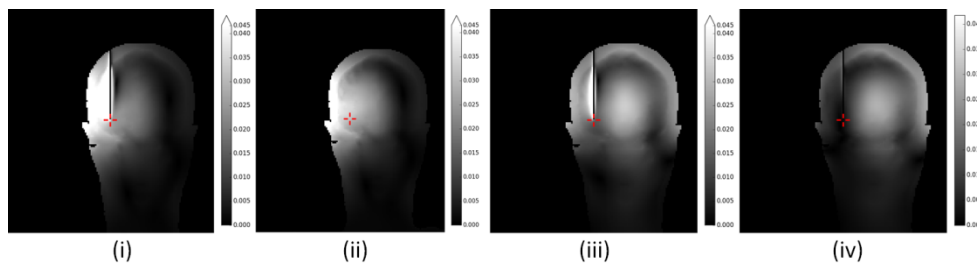


Fig.1: Coil model with 'Ella' and implanted wire, shield removed for better visibility.

Fig.2: Coronal maps of $|B_1^+|$ in μT for configuration (i) - (iv) (total forward power = 2.5 mW). $|B_1^+|$ artifacts near the implant are due to induced RF currents. In configuration (iv) these artifacts are effectively suppressed. The red cross indicates the position of the wire's tip.



	psSAR _{10g} in W/kg	T _{tip} in °C	T _{csf} in °C
(i)	43.4	41.3	41.4
(ii)	43.6	37.9	39.2
(iii)	11.7	38.2	38.7
(iv)	17.5	37.3	37.8

Tab.1

Fig.3: Coronal maps of steady state temperature for configuration (i) - (iv) (total forward power = 20 W). Different temperature scales are for better visibility. The red cross indicates the position of the wire's tip.

Results and Discussion: From calculated $|B_1^+|$ - maps (s. Fig.2) it is obvious that induced RF currents in the wire can effectively suppressed by the proposed method (iv) whereas the $|B_1^+|$ distributions remains feasible for spin excitation. The thermal simulations (s. Fig.3) reveal that for configuration (i) and (ii), i.e. when using the 'worst case' voltage vector $|u_{max}\rangle$, peak values of spatial SAR of > 40 W/kg occur (s. Tab. 1) which result in maximum tissue temperatures > 42.5°C even when no implant is present. Nevertheless, T_{tip} is clearly enhanced when the wire is present (41.3°C compared to 37.9°C). A similar behavior is found for the more 'benign' CP-mode (iii) whereas for configuration (iv) no significant heating due to the implant can be observed proving the efficacy of the approach (s. Tab.1).

Conclusion: We have shown for a 7T transmit head coil array that a single Q matrix Q_{imp} associated with a conductive implant is sufficient to describe tissue heating nearby the implant. Since the largest eigenvalue of Q_{imp} dominates all the other, a projection to an orthogonal sub space can be applied to construct steering conditions which minimize the hazards of implant heating. As a result the degrees of freedom for optimization of B_1^+ are restricted only marginally.

Acknowledgments: This work was supported by EMRP grant HLT06. The EMRP is jointly funded by the EMRP participating countries within EURAMET and the European Union.

References: 1. M. Murbach *et al.*, MRM 71 (2014) 421-431. 2. A. Christ *et al.*, 2010 Phys. Med. Biol. 55 N23, doi:10.1088/0031-9155/55/2/N01. 3. www.itis.ethz.ch/itis-for-health/tissue-properties/database.